Failure Mode Classification of IGBT Modules Under Power Cycling Tests Based on Data-Driven Machine Learning Framework

Xin Yang, *Senior Member, IEEE*, Yue Zhang, Xinlong Wu, and Guoyou Liu, *Senior Member, IEEE*

***Abstract*—Of great significance is knowledge of failure modes of IGBT modules under power cycling test (PCT) in advance. It can not only precisely determine accurate utilization of physics-of-failure lifetime prediction methods but also help optimize IGBT designs. However, establishing an accurate and generic offline failure mode classification method for different IGBT modules remains a challenging problem due to the complex degradation process of IGBT modules. In this article, a data-driven convolutional neural network (CNN) based method is proposed for quad-classification of failure modes for different IGBT modules under different PCT conditions. First, in order to accurately characterize the mapping between the failure modes and the precursor parameters, a framework of precursor parameters is meticulously established. Then, mainly using collected training data from existing publications, the CNN classification model is developed by a newly dynamic tuning-multilevel particle swarm-back propagation optimization algorithm. Finally, experimental PCTs of various IGBT modules are performed. The obtained PCT data and additional testing data from existing publications are used to verify the generalizability and robustness of the proposed classification method. The superiority of the proposed method is well demonstrated through comparison with random CNN, the state-of-the-art particle swarm optimization CNN, and other intelligent algorithms.**

***Index Terms*—Convolutional neural network (CNN), data-driven, failure mode, IGBTs, multilevel particle swarm (MPS).**

I. Introduction

IGBTS have been widely used in aerospace, automotive, railway transportation, wind plant, etc. [1]. Therefore, more demanding requirements are imposed on IGBT module manufacturers that IGBT modules must have high reliability to ensure safe and stable operation of power electronic systems.

Manuscript received 6 March 2023; revised 22 May 2023, 28 July 2023, and 30 August 2023; accepted 8 September 2023. Date of publication 12 September 2023; date of current version 23 October 2023. This work was supported in part by the National Natural Science Foundation of China under Grant 52077071 and in part by Provincial Natural Science Foundation of Hunan under Grant 2022JJ30150. Recommended for publication by Associate Editor K. Ngo. *(Corresponding author: Yue Zhang.)*

Xin Yang is with the College of Electrical and Information Engineering, Hunan University, Changsha 410082, China, and also with the Engineering Research Center of Advanced Semiconductor Technology and Application of Ministry of Education, Hunan University, Changsha 410082, China (e-mail: xyang@hnu.edu.cn).

Yue Zhang and Xinlong Wu are with the College of Electrical and Information Engineering, Hunan University, Changsha 410082, China (e-mail: zy19573134037@hnu.edu.cn; wxl820@hnu.edu.cn).

Guoyou Liu is with CRRC Zhuzhou Electric Locomotive Institute Company Ltd., Zhuzhou 412000, China (e-mail: liugy@csrzic.com).

Color versions of one or more figures in this article are available at https://doi.org/10.1109/TPEL.2023.3314738.

Digital Object Identifier 10.1109/TPEL.2023.3314738

In order to ensure that the IGBT modules can reliably operate in practical applications, it is necessary to evaluate reliability of IGBT modules. An important part of reliability evaluation of IGBT modules is to perform lifetime prediction under power cycling tests (PCTs). The results of lifetime prediction can help manufacturers better evaluate reliability of IGBT modules, and also help manufacturers to optimize the structure and design parameters of IGBT modules, so as to extend the service lifetime of IGBT modules. The aging data generated from PCTs are widely used for the development of empirical lifetime prediction models [2], [3]. The empirical lifetime prediction models are the most widely used method for lifetime prediction of IGBT modules, including Coffin–Manson model, Coffin–Manson–Arrhenius model, Bayerer model, etc. [4], [5]. However, there is a serious issue for these models. Abuelnaga et al. [6] reported that these lifetime prediction models are derived on the basis of one key assumption that each failure mode is completely independent. Hanif et al. [5] reported that due to different test protocols and module types, the dominant failure modes, observed for different IGBT modules, are different. Yang et al. [4], Pedersen and Pedersen [7], and Lu and Christou [8] reported that the lifetime prediction model fitted from the historical data from PCTs cannot be applied to different PCT conditions. If the failure mode of the used lifetime prediction model disagrees with the failure mode of the actual PCT condition, the lifetime prediction model will produce abnormal results [9]. For these reasons, different failure modes require different empirical lifetime prediction models. For example, the empirical lifetime prediction model derived from the solder fatigue data is inapplicable to predict the IGBT lifetime resulted by bond wire failure. Therefore, when manufacturers need to perform lifetime prediction under a certain testing condition, they first need to estimate what failure mode of IGBT modules will occur under this testing condition. In this way, the application of the lifetime prediction model has a high degree of credibility and applicability. However, until now, there are little known mathematical models or physical models that allow us to predict the failure modes of IGBT modules under a given PCT condition.

It is very challenging to accurately predict the failure mode of an IGBT module under a given PCT condition. Multiple contributors need to be considered, which will make the reliability evaluation task more difficult [10]. The work in [11], [12], and [13] also mentioned that there exist several substantial competing factors, for example, contributing to the degradation of the solder

joints or bond wires. Absolute separation between the different failure modes is difficult [14]. The existence of different failure modes means that the coupling between the different failure modes is very complex. That is, there is a particularly complex mapping relationship between the precursor parameters and the failure modes.

Machine learning is able to bridge a meaningful correlation among the precursor parameters and failure modes under different testing conditions [11]. And among many machine learning algorithms, convolutional neural networks (CNNs) have demonstrated high recognition performance for large-scale classification tasks [15]. The work in [16] and [17] also mentioned that classification and feature extraction have been the most important applications of CNN. Not only that, CNN is one of the most popular deep-learning-based fault classification methods [18]. For example, power quality event classification [17], bearing fault diagnosis [19], IGBT open-circuit fault diagnosis [20], various industrial process fault diagnosis [21], etc. However, adopting CNN for package failure mode classification of IGBT modules under PCTs remains unexplored. In order to fill this gap, this article proposes a CNN-based failure mode classification method to achieve accurate failure mode classification for different IGBT modules.

Hyperparameter optimization is crucial for the performance of CNN. The performance of CNN heavily depends on their hyperparameters [18]. The default hyperparameters cannot guarantee the final performance of CNN [22], which makes the hyperparameter tuning process very essential for the application of CNN on failure mode classification. Particle swarm optimization (PSO) is the most preferred choice in solving optimization problems because it has fewer parameters, simpler formulation, and is easier for computation [23]. However, the different failure modes and the precursor parameters have the complex and tight coupling. This makes it difficult for the standard PSO to obtain the optimal CNN hyperparameters. An improved PSO is required.

In this regard, some scholars have studied the optimization of hyperparameters under pregiven the overall architecture of the CNN [24], [25]. The overall architecture refers to the number of convolution layers, pooling layers, and fully connected (FC) layers. The disadvantage of this approach is that the overall architecture of the CNN needs to be manually pregiven, which strongly relies on one's understanding of the empirical knowledge on CNN. If the given overall architecture is unreasonable, it will be difficult to obtain a well-performing CNN classification model in the end. Other scholars generate entirely new CNN from scratch [23], [26]. Their goal is to optimize the hyperparameters in a broad sense, such as the number of layers, the learning rate, etc. The advantage of this approach is that it requires less manual effort and is able to automatically perform CNN architecture search and hyperparameters optimization.

Therefore, in this article, an offline data-driven CNN-based classification model that has both optimal architecture and hyperparameters is developed. The rest of this article is organized as follows. In Section II, detailed preparation work of training data is presented. Section III described the implementation steps of the CNN hyperparameter optimization method and the associated optimization results. In Section IV, PCTs were implemented and corresponding results are shown. The generalizability and robustness of the proposed classification model will be verified by these data. The superiority of the proposed classification method will be demonstrated through the comparison with random CNN and the state-of-the-art PSO-CNN. Finally, Section V concludes this article.

II. Offline Data-Driven Classification Model

A. Precursor Parameter Framework Establishment

In order to accomplish the accurate failure mode classification of IGBT modules, a generic and comprehensive precursor parameter framework is needed. The package failure is the most frequently observed in wire-bonded IGBT modules [27]. Therefore, this article focuses on finding the precursor parameters related to the package failure in this article.

1) Dimensional Parameters: First, the literature [28] found that increasing the bond wire aspect ratio α shifts the failure mode from heel crack toward lifting-off under PCTs. Second, 3-D finite element analysis was performed in the literature [29] to investigate the influence of different bond wire diameters D on the thermos-mechanical reliability. By performing numerical Ansys 2-D device simulations, Wang et al. [30] pointed out that as the chip plane size (the product of the length L_1 and width W_1 of the chip) decreases, the heat dissipation capability will rapidly decrease, which will lead to a subsequent increase in junction temperature and aggravate the aging failure of the IGBT module. Similarly, Poech [31] and Junghaenel et al. [32] pointed out that the thinner the Si chip h_1, the more important is the influence of underlying layers for the thermal expansion of the die's surface. As a consequence, Al wires have a higher lifetime on thinner Si chips as these can more easily follow the thermal expansion of the substrates. Finally, by performing a set of PCTs, Ma et al. [33] pointed out that the failure rate of solder joints is largely influenced by the geometry of the solder joints, i.e., solder layer length L_2, solder layer width L_2, and solder layer thickness h_2. In summary, the bond wire aspect ratio α, bond wire diameter D, chip length L_1, chip width W_1, chip thickness h_1, solder layer length L_2, solder layer width W_2, and solder layer thickness h_2 mentioned earlier are regarded as dimensional parameters.

2) Materials Parameters: It is well known that the wire-bonded IGBT modules have a multilayer physical structure [34]. Different materials have different coefficient of thermal expansion (CTE). It is the presence of the CTE mismatch that causes the appearance of solder layer fatigue and bond wire failure. The cross-sectional view of the IGBT module (SKM100GB12T4 as an example) is given in Fig. 1.

Therefore, during a PCT, the mismatch between the CTE of the internal layers of the IGBT module will render each layer withstanding repeated alternating thermal stresses. This eventually leads to cracks in the solder layer; bond wires are subjected to interface shear and lifting-off of bond wires occurs; bond wires are subjected to temperature cycling, repetitive expansion and contraction, and heel cracking of bond wires occurs [34]. Therefore, the CTE difference between the bond wire and the chip, and the CTE difference between the chip and the solder layer all have a certain degree of influence on the fatigue of the

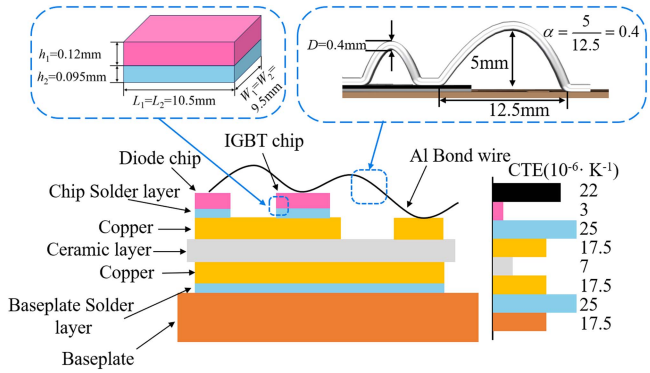

Fig. 1. Cross-sectional view of the IGBT module.

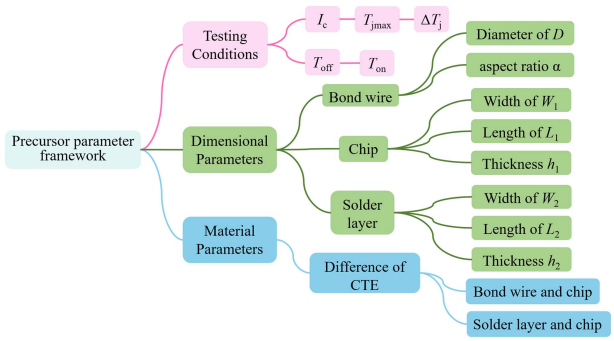

Fig. 2. Precursor parameter framework in the form of a tree diagram.

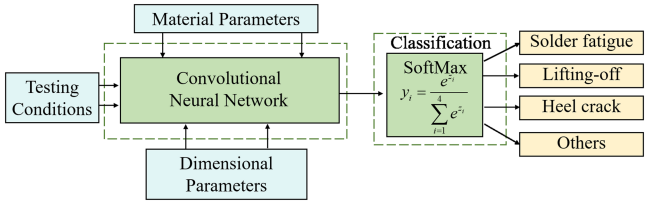

Fig. 3. Work framework for establishing mapping relationship.

IGBT module. These two CTE differences are called material parameters.

3) PCT Conditions: Similarly, the package failure of IGBT modules is caused by the thermomechanical fatigue stress during the PCT [7]. The amplitude and duration of thermomechanical fatigue stress are closely related to the testing conditions of the PCT, including junction temperature fluctuation ΔT_j, maximum junction temperature T_{jmax}, turn-ON time t_{on}, turn-OFF time t_{off}, and load current I_c. These five parameters mentioned earlier are testing conditions.

The precursor parameter framework is presented in the form of a tree diagram, as shown in Fig. 2. In total, there are 13 precursor parameters. Each precursor parameter is a given value. Our work is to establish the mapping relationship between these precursor parameters and the failure modes of the IGBT module, as shown in Fig. 3. It should be noted that the word "others" in the Fig. 3 refers to the occurrence of severe degradation of both bond wire and solder layer.

B. Dynamic Tuning-Multilevel Particle Swarm-Back Propagation (D-MPS-BP) Optimization Algorithm

In this article, we try to find optimal hyperparameters to develop an offline data-driven CNN-based classification model. A typical CNN classification model consists of at least four different layers namely the convolutional layer, pooling layer, FC layer, and softmax layer [21]. This CNN classification model is developed based on MATLAB and the corresponding computer configuration is: Intel(R) Xeon(R) 8375C CPU @ 2.90 GHz, 32 cores, 64 threads, and 128.00-GB RAM.

To better optimize CNN hyperparameters and avoid the high cost of manual effort, the multilevel particle swarm (MPS) optimization algorithm that can automatically search for CNN architecture and hyperparameter configurations is clearly required. A D-MPS-BP optimization algorithm is newly developed. The dynamic tuning strategy adopts sigmoid decreasing inertia weight and linearly decreasing learning factors [23], [25]. This is also used to avoid local optimal during the optimization process.

The MPS is derived from Singh et al. [23] and Tian and Shi [26]. The particle swarm finds the optimal number of convolution layers, pooling layers, and FC layers at level-1 by exploring the search space that has been predefined with a maximum number of layers. We refer to the number of layers in each layer as level-1 hyperparameters. A nonlinear activation function is usually applied immediately after each convolutional layer.

Then, the particle swarm finds the optimal set of hyperparameters of each layer at level-2 by exploring the search space where hyperparameters have been predefined with a maximum value. We refer to the number of convolution filters, convolution filter size, convolution stride size, pooling filter size, pooling stride size, Adam algorithm learning rate, first moment vector, second moment vector, and the number of neurons for each FC layer as level-2 hyperparameters.

The BP algorithm and Adam gradient descent algorithm are used to update the filter coefficients, FC neural network weights, and biases [35]. We refer to the aforementioned hyperparameters as level-3 hyperparameters. In addition, the weights and biases are initialized with Xavier [36] and zeros, respectively. And the loss function is the cross-entropy loss function [37].

In each given level-1 and level-2 hyperparameters space, the BP algorithm is utilized to iteratively search for the optimal set of level-3 hyperparameters. For the optimization of level-3 hyperparameters, there are also many researchers aiming to utilize the PSO to find optimal configurations [38], [39], [40]. However, the level-3 hyperparameters can be optimized with just a few BP epochs rather than using the PSO. This is a joint search-type hyperparameter optimization method.

The hierarchical structure of particle swarms at level-1 and level-2 is shown in Fig. 4. Each particle at level-1 possesses three dimensions, corresponding to the level-1 hyperparameters. Each particle in level-2 possesses $8+c$ dimensions (c is the number of FC layers), which corresponds to level-2 hyperparameters. For each particle, each of its dimensions possesses a personalized speed limitation when updating its position and velocity. Fig. 5 shows the flowchart for optimizing

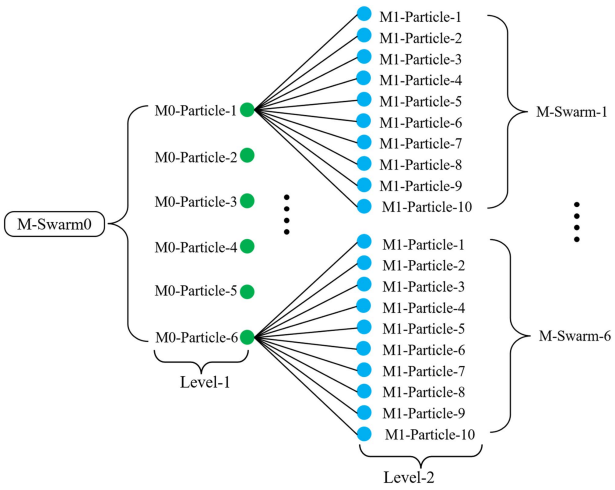

Fig. 4. Hierarchical structure of swarms at level-1 and level-2.

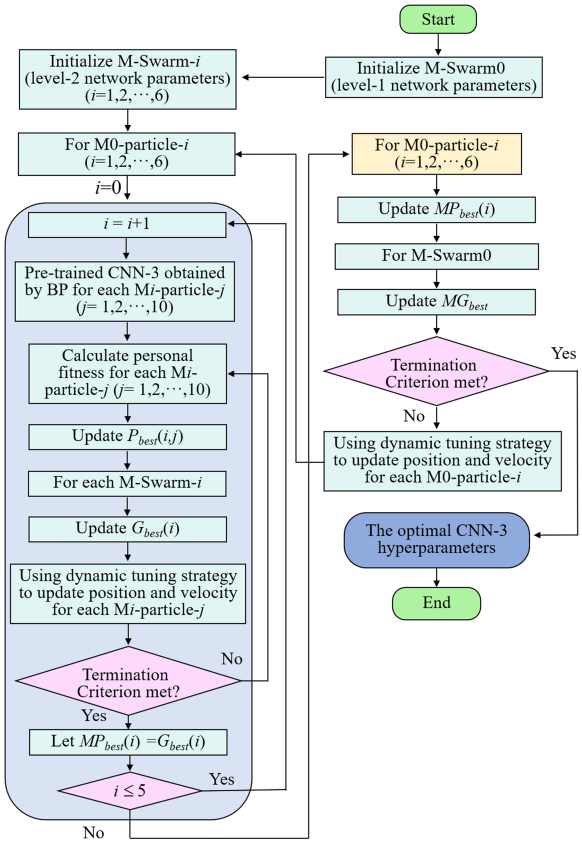

Fig. 5. Flowchart for optimizing the CNN-3 hyperparameters using the D-MPS-BP optimization algorithm.

the CNN-3 hyperparameters using the D-MPS-BP optimization algorithm.

III. Data Collection and Validation

A. Data Collection

Enriching collection of relevant training data is also the basis for subsequent training of the CNN with optimal results. In our work, most of the training data collected are from existing publications [2], [27], [28], [29], [32], [41], [42], [43], [44], [45], [46], [47], [48], [49], [50], [51], [52], [53], [54], [55], [56], [57], [58], [59], [60], [61], [62]. Each set of training data contains 13 precursor parameters.

First, more attentions are paid to diversification of training data during the data collection process. The training data contain PCT data of various different IGBT modules (e.g., SKM200GB12T4 module, SKM50GB12T4 module, GD50HCU120B3S module, FS150R12KT4 module, FS200R07A1E3 module, etc.) under different testing conditions. The advantages are as follows. First, it provide enough information to train the CNN classification model. Second, it enables the proposed method robust enough to apply to different IGBT modules.

Second, it should be noted that during the collection of training data from existing publications, the failure criterion of the solder fatigue is a 5% increase in thermal resistance R_{th}, and the failure criterion of the bond wire is a 20% increase in collector–emitter saturation voltage V_{ce}. A total of 147 sets of training data are collected from existing papers, 49 sets of which are used for validation. Among the training sample set, the sample numbers of solder fatigue, bond wire lifting-off, bond wire heel crack, and "others" are 37, 49, 5, and 7, respectively; the percentages of the four are: 37.76%, 50.00%, 5.1%, and 7.14%, respectively.

Finally, it should be noted that there is a problem called training database imbalance. This is because the number of samples of the bond wire heel crack and "others" in training sample set is much smaller compared to the other two categories. Existing research on the database imbalance problem has concentrated mainly on two levels: the data level and the algorithmic level [63]. In our classification task, it is preferred to retain useful information about the majority class data and add useful information about the minority class. In addition, the adjustment process is required to easily operate and observe, and not to introduce new parameters nor add redundant computational effort. Based on the aforementioned considerations, oversampling techniques are expected to become our friendly choice.

Oversampling technology is to reach a desired level of balance by randomly copying minority samples [63]. For unbalanced categories, the sample set size is increased by randomly copying existing samples. Eight sets of bond wire heel crack samples are randomly copied as well as ten sets of "others" samples. After this, the sample numbers of solder fatigue, bond wire lifting-off, bond wire heel crack, and "others" become 37, 49, 13, and 17, respectively; and the percentages of the four are: 31.9%, 42.24%, 11.21%, and 14.66%, respectively. Now, 165 sets of training data from existing papers are established, 49 sets of which are still used for validation.

B. Data Preprocessing

Different precursor parameters within the CNN usually have different measurement units and different ranges. Therefore, in order to eliminate the effects of the difference in unit and range, the precursor parameters are needed for preprocessing. Here,

TABLE I
RESULTS OF ONE-HOT ENCODING

Failure mode	Solder fatigue	Heel crack	Lifting-off	Others
encoding form	[1 0 0 0]	[0 1 0 0]	[0 0 1 0]	[0 0 0 1]

the data scaling method is used. The min–max scaling formula is employed to scale the precursor parameter into a predefined range of [0.1, 0.9] [12].

For the output results (i.e., the main package failure modes of the IGBT modules: solder fatigue, bond wire lifting-off, bond wire heel crack, and "others" [41]), which are in text form and cannot be directly input into the CNN. To use them during the CNN training process, we need to digitalize them first. To convert the failure modes into an easy form to perform multiclassification task, one-hot coding method is introduced to encode failure modes into a vector space [64]. In our work, one-hot encoding is presented as a four-digit binary encoding. The results of one-hot encoding are given in Table I.

Next, to better illustrate the superiority of the newly proposed hyperparameter optimization algorithm for our classification problem. The validation sample set is used to compare the random CNN, state-of-the-art PSO-CNN, and newly optimized CNN in terms of classification accuracy. There are 49 sets of validation samples in validation sample set.

C. Comparison

1) Random CNN: The random generated CNNs are initialized with the same random set of hyperparameters as in the D-MPS-BP model for a fair comparison of performance. Ten CNNs are randomly generated. All padding pixels are set to zero.

A random CNN is generated with the best classification results and it is called the best random CNN. The validation results of the best random CNN are given in Fig. 6(a). The validation accuracy is only 57.14%. The classification accuracy by random CNNs is very low. This is because the hyperparameters of best random CNN are given randomly. The time consumption of training best random CNN is 15.5571 s.

2) State-of-the-Art PSO-CNN: To obviously illustrate the disadvantage of optimizing hyperparameters under pregiven overall architecture of the CNN, the validation accuracies of CNN-1 and CNN-2 are compared. CNN-1 uses random architecture and CNN-2 uses the localized architecture obtained by the trial-and-error method. A localized architecture means that the numbers of convolution and pooling layers are given manually, whereas the number of FC layers is unknown. Set the number of convolutional layers to 1 and the number of pooling layers to 1. Therefore, the trial-and-error method is used to explore the optimal number of FC layers. The search range is [1 5]. A total of five trial and errors are required.

The state-of-the-art PSO in [25] is used to optimize the hyperparameters of CNN-1 and CNN-2. This state-of-the-art PSO improves the standard PSO by using nonlinear inertia weight and

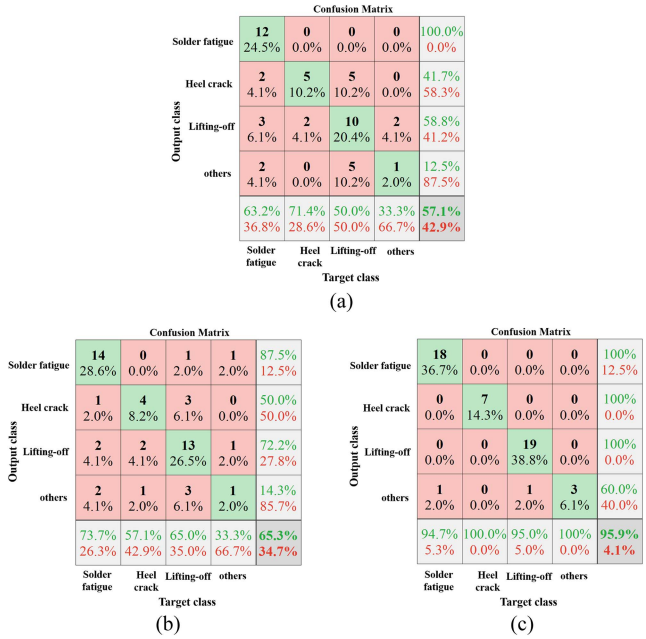

Fig. 6. Validation results. (a) Best random CNN. (b) CNN-1. (c) CNN-2.

linearly decreasing learning factors. The number of misclassified samples in the validation phase is used as the fitness function. We set up a total of 20 iterations. Record the time consumption of training for 20 iterations. The time consumptions of training CNN-1 and CNN-2 took 10352.6 s and 48430.5 s, respectively.

The validation results and testing results of CNN-1 and CNN-2 are given in Fig. 6(b) and (c). The validation accuracies of CNN-1 and CNN-2 are 65.3% and 95.9%, respectively. It can be found that the pregiven CNN architecture will largely affect the final classification accuracy. The classification accuracy of CNN-2 is higher than CNN-1. This is because the CNN-1 architecture is given randomly without involving too much manual effort. Then, if one wants to give a reasonable CNN architecture before hyperparameter optimization, the cost of manual effort will be much higher.

3) D-MPS-BP Convolutional Neural Network: Table II gives the optimal level-1 and level-2 hyperparameters of CNN-3 that are optimized by D-MPS-BP optimization algorithm. Fig. 7 gives the architecture of the proposed CNN-3 classification model.

The validation results of CNN-3 are given in Fig. 8. The validation accuracy is 98%. Fig. 9 gives the curves of the best global fitness with the number of iterations during the optimization process. From Fig. 9, it is found that the D-MPS-BP CNN-3 finally got a better global fitness than the CNN-2 and CNN-1. When the number of iterations is greater than 18, the global fitness curve of D-MPS-BP CNN-3 trends to a constant. The number of BP epochs is set to 15. Fig. 10 gives the curve of the loss function with BP epoch during the optimization of level-3 hyperparameters for CNN-3 when the number of iterations is 18. When the epoch is greater than 12, the loss function corresponding to each failure mode converges and tends to zero.

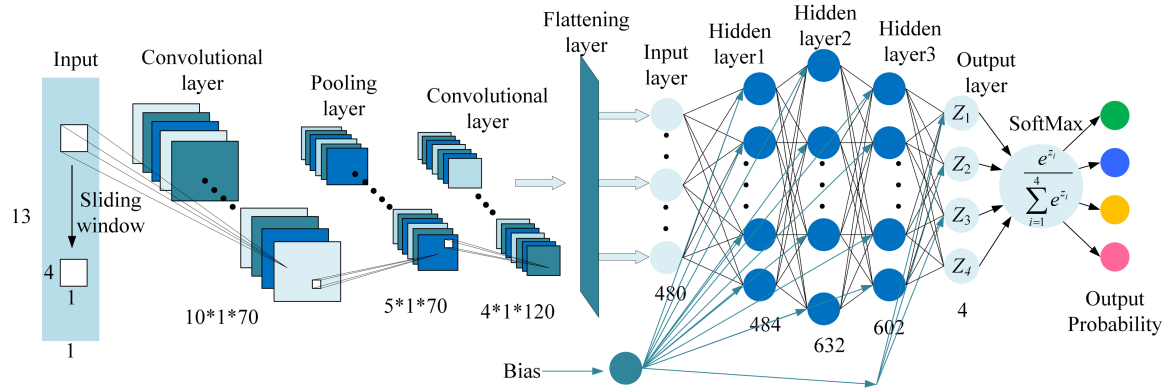

Fig. 7. Architecture of the proposed CNN-3 classification model.

TABLE II
OPTIMAL LEVEL-1 AND LEVEL-2 HYPERPARAMETERS OF CNN-3

	Hyperparameter	Range	Maximum speed	CNN-3
Level-1	convolution layers	[1 5]	1	2
	pooling layers	[1 5]	1	1
	FC layers	[1 5]	1	3
Level-2	convolution filters	[10 100]	5	filter1: 70 filter2: 55
	convolution filter size	[1 5]	1	filter1: 4 filter2: 2
	convolution stride size	[1 5]	1	filter1: 1 filter2: 1
	pooling filter size	[1 5]	1	2
	pooling stride size	1 5]	1	2
	Adam algorithm learning rate	[0.001 0.02]	0.001	0.0124
	First moment vector	[0.90 0.95]	0.001	0.924
	Second moment vector	[0.95 0.999]	0.001	0.973
	Number of neurons	[1 1024]	20	484 632 602

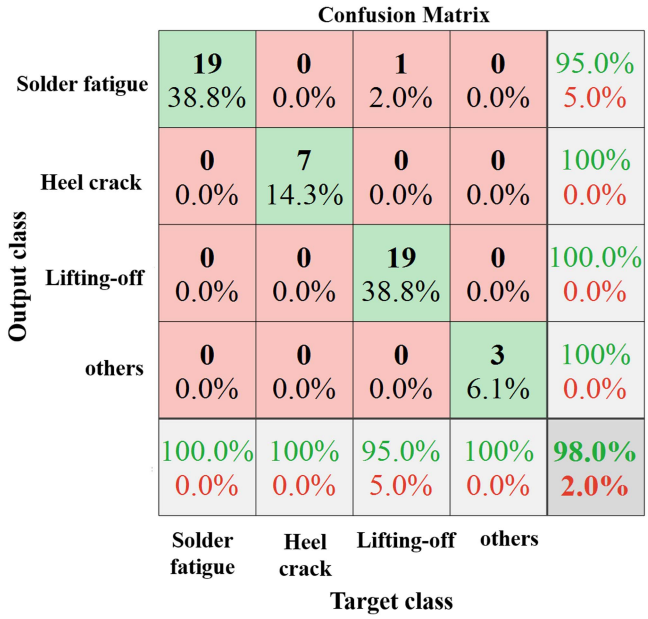

Fig. 8. Validation results of CNN-3.

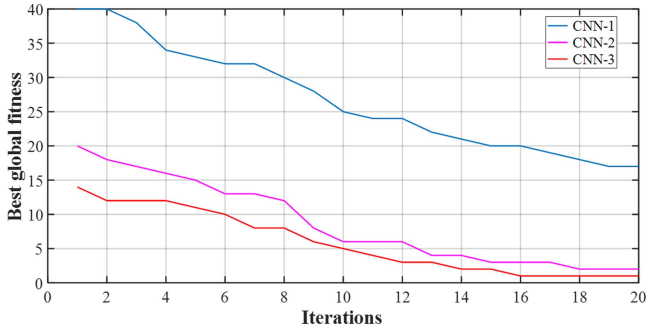

Fig. 9. Curves of the global fitness with the number of iterations.

This means that under the level–1 and level–2 hyperparameters space at an iteration number of 18, the level–3 hyperparameters are relatively optimal.

Using validation accuracy and time consumption of training as comparison indicators, the best random CNN, CNN-1, CNN-2, and CNN-3 are compared. We also provide comparisons with other intelligent algorithms, such as PSO extreme learning machine (ELM) [65] and Gini index decision tree (DT) [66]. Table III lists corresponding comparison results.

First, the best random CNN has the shortest training time, but the validation accuracy is extremely low. Second, the validation accuracy of CNN-1, which uses a random architecture for hyperparameter optimization, is only moderately improved relative to the best random CNN. This illustrates that if the CNN uses a random architecture for hyperparameter optimization, the final result is not guaranteed either. Third, comparing CNN-2 and CNN-1, the validation accuracy of CNN-2 is significantly improved, but the time consumption of training incurred is huge. Finally, comparing CNN-3 and CNN-2, it can be seen that the validation accuracy of CNN-3 is improved, and its time consumption of training is also drastically reduced. For PSO-ELM

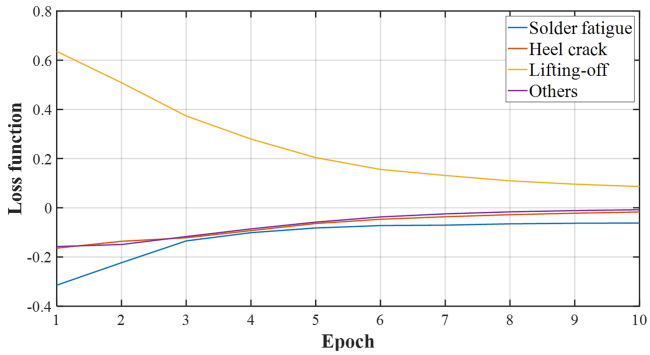

Fig. 10. Curve of the loss function with BP epoch during the optimization of level-3 hyperparameters for CNN-3 when the number of iterations is 18.

TABLE III
VALIDATION ACCURACY AND TIME CONSUMPTION COMPARISONS BETWEEN DIFFERENT ALGORITHMS

Optimizer	Intelligent Algorithms	Validation accuracy	Time consumption of training
none	Best Random CNN	57.1%	15.5571s
The state-of-the-art PSO	CNN-1	65.3%	10352.6s
	CNN-2	95.9%	48430.5s
D-MPS-BP	CNN-3	98%	31206.6s
PSO	ELM	89.8%	6.652s
none	Gini index DT	83.7%	1.636s

and Gini index DT, although both have certain advantage in terms of time consumption, their classification accuracies are lower than that of CNN-3. The superiority of the D-MPS-BP optimization algorithm in solving the classification problem is fully demonstrated.

IV. EXPERIMENTAL TEST

A. Accelerated PCT

In order to verify the generalizability and robustness of the CNN-3 classification model, a testing sample set is created. The testing sample set consists of two parts. First, performing accelerated PCT for different modules under different testing conditions, the part1 testing sample set can be obtained. Second, a small portion of the PCTs data in the existing publications [42], [43], [44], [45], [46], [47], [48] is used for part2 testing sample set.

Fig. 11 shows the test rig, which consists of the circuit part and water cooling part. The circuit part includes the main circuit, control circuit, driving circuit, and measurement circuit; the water-cooling part includes the water-cooling machine, water-cooling plate, and water return pipes. Fig. 12 shows the main electrical circuit of the rig. The 50-mA current source within it is used to execute the temperature-sensitive electrical parameter method to measure the value of V_{ce} [67]; and the NI-DAQ is a data acquisition card with the model number NI USB-6341.

After designing and building test rig, the devices under test (DUT) can be selected. Four different types of IGBT modules

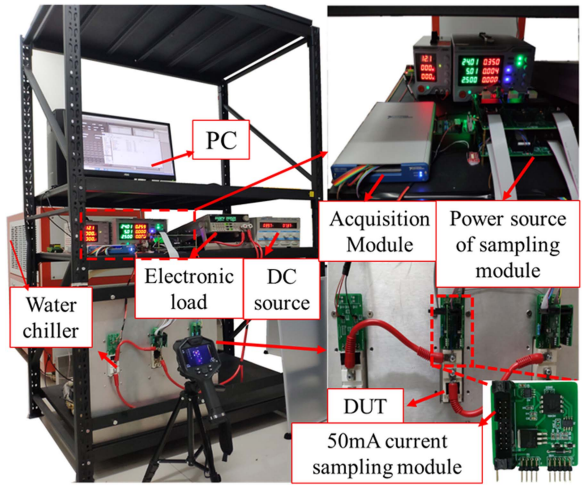

Fig. 11. Physical view of the PCT rig.

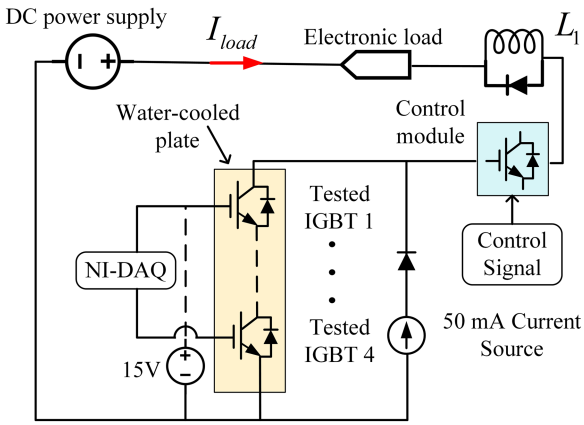

Fig. 12. Main electrical circuit of the PCT rig.

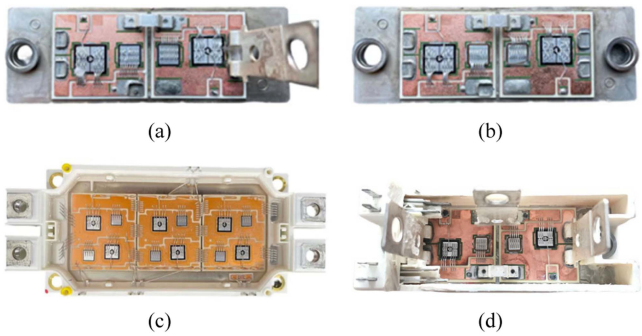

Fig. 13. Tested IGBT modules. (a) FF100R12RT4(FF100) module. (b) SKM100GB12T4(SKM100) module. (c) FF150R12ME3G(FF150) module. (d) SKM50GB12T4(SKM50) module.

are used, as shown in Fig. 13(a)–(d). The advantage of choosing different types of IGBT modules is to enrich and diversify the testing sample set. The testing conditions are shown in Table VI, which gives the load current I_c, turn-ON time t_{on}, turn-OFF time t_{off}, junction temperature fluctuation ΔT_j, and maximum junction temperature T_{jmax} for each IGBT module

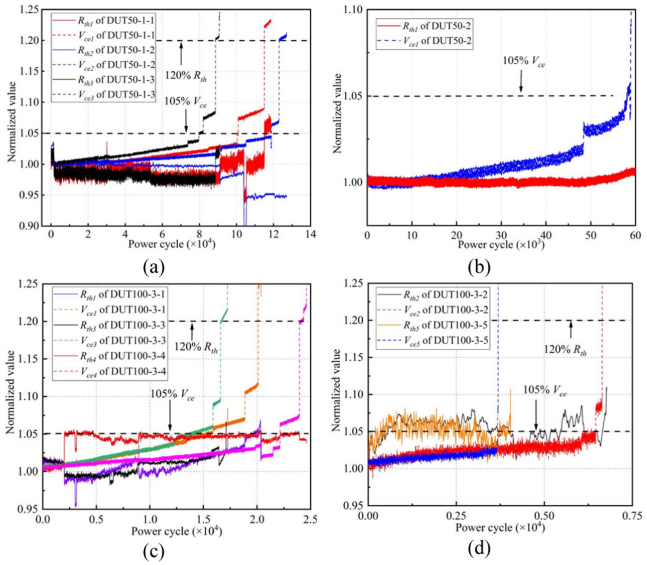

Fig. 14. Evolution curves of $R_{\rm th}$ and $V_{\rm ce}$ throughout the PCT aging process. (a) DUT50-1 series. (b) DUT50-2 series. (c) DUT100-3series. (d) DUT100-3 series.

during the PCT. Table VI is placed in the Appendix. A total of 35 IGBT modules will be tested. The DUT50 series are all SKM50 modules, the DUT150 series are all FF150 modules, the DUT100-1 and DUT100-2 series are all SKM100 modules, and the DUT100-3 series are all FF100 modules.

B. Analysis of Aging Results

1) Bond Wire Failure: Fig. 14 shows the evolution curves of $V_{\rm ce}$ and $R_{\rm th}$ throughout the PCT. $V_{\rm ce}$ and $R_{\rm th}$ are used to monitor bond wire failure and solder layer fatigue, respectively. The curves in Fig. 14 were actually measured during our PCTs. The predefined failure criteria of bond wire failure and solder layer fatigue are 5% increase of $V_{\rm ce}$ and 20% increase of $R_{\rm th}$, respectively [67]. As it can be seen in Fig. 14(a)–(d), $V_{\rm ce}$ first rose to 1.05 times its initial value. This initially determine that bond wire failure first occur.

In order to further determine the failure modes of the DUTs, it is necessary to examine inside of the module with the help of certain instruments. The DUT50-1, DUT50-2, and DUT100-3 modules were uncased. A microscope was used to observe the bond wires. It was found that the bond wires were obviously lifting-off, as shown in Fig. 15(a) and (b).

Unfortunately, the bond wire heel crack did not appear in the PCTs that we performed. This is because the packaging technology and bonding process of IGBT modules are now considerably improved [42], [68], [69]. However, these data are supplemented by utilizing heel crack data from existing publication [42]. Fig. 15(c) shows the image of bond wire heel crack in paper [42].

2) Solder Layer Fatigue: Fig. 16 shows the evolution curves of $V_{\rm ce}$ and $R_{\rm th}$ throughout the PCT aging process. As it can be seen in Fig. 16(a)–(f), $R_{\rm th}$ first rose to 1.2 times its initial value. This initially determine that the solder layer fatigue first occur.

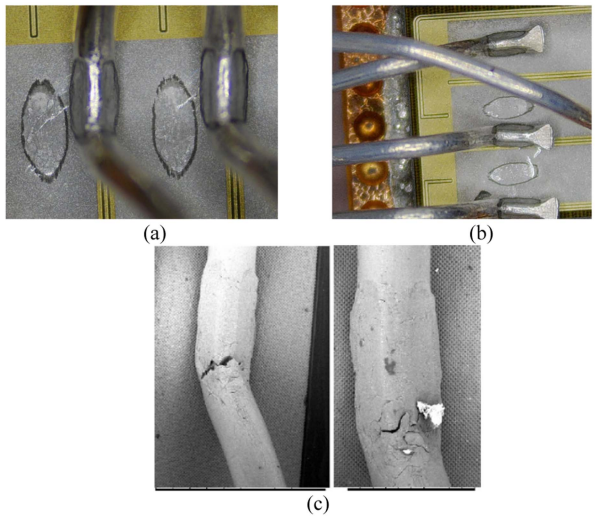

Fig. 15. Images of bond wire failure. (a) Bond wire lifting-off of DUT50-1 and DUT50-2. (b) Bond wire lifting-off of DUT100-1. (c) Bond wire heel crack [42].

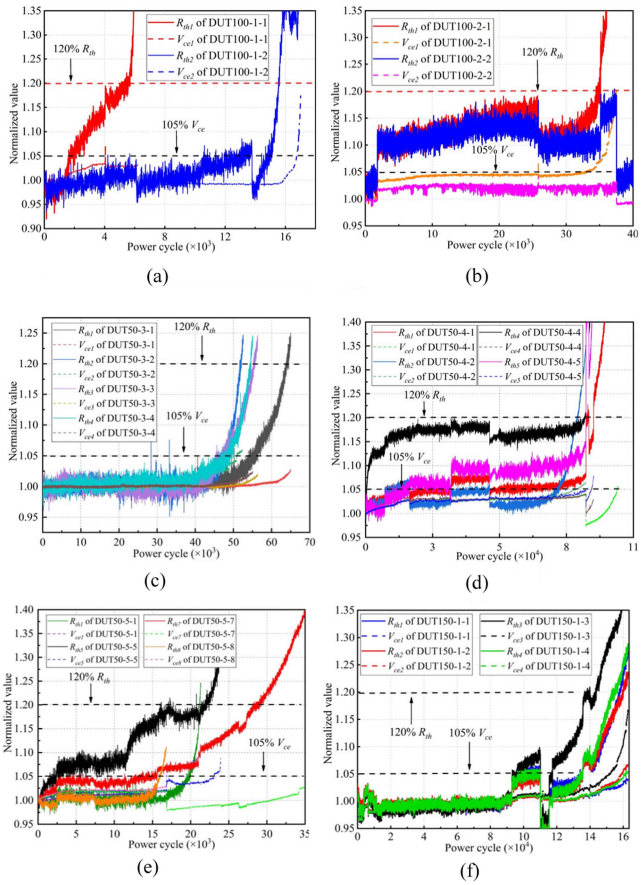

Fig. 16. Evolution curves of $R_{\rm th}$ and $V_{\rm ce}$ throughout the PCT aging process. (a) DUT100-1 series. (b) DUT100-2 series. (c) DUT50-3series. (d) DUT50-4 series. (e) DUT50-5 series. (f) DUT150-1 series.

The chip solder layers of the DUT100-1, DUT100-2, DUT50-3, DUT50-4, and DUT50-5 IGBT modules were scanned using computed tomography (CT), and the chip solder layer of the DUT150-1 modules was scanned using scanning acoustic microscopy (SAM). All scanned results are shown in Fig. 17.

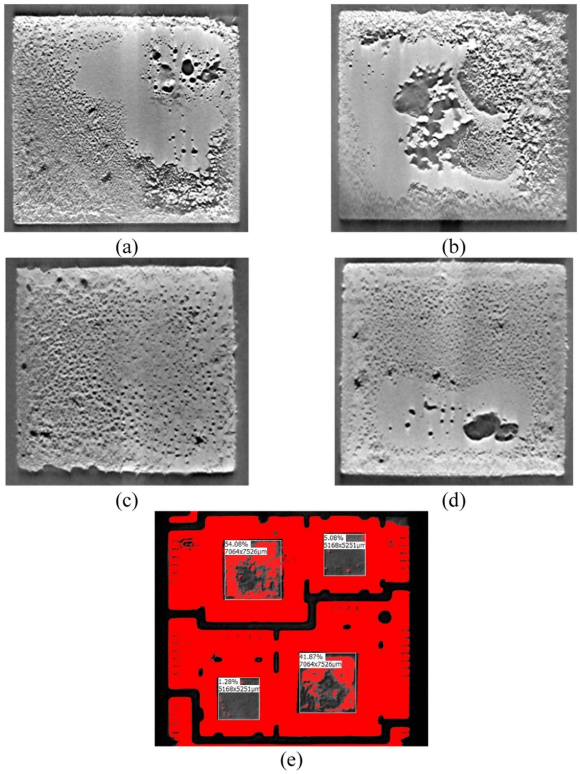

Fig. 17. Scanned results. (a) DUT50-3 solder layer. (b) DUT50-4 solder layer. (c) DUT50-5 solder layer. (d) DUT100-1 and DUT100-2 solder layers. (e) DUT150-1 solder layer.

Fig. 17(a)–(d) shows the CT images, and Fig. 17(e) shows the SAM images. As shown in Fig. 17, there are visible chip solder degradations.

3) Others: This mode indicates the occurrence of severe degradation of both bond wire and solder layer. Some data are obtained as supplemental testing samples [43], [44], [45], [46], [47], [48].

It should be noted that these PCT curves are not the input data of CNN. The input data of CNN are the precursor parameters given in Section II-A.

C. Testing CNN-3 Classification Model

After performing PCTs on the DUTs under the given testing conditions, the corresponding failure modes are obtained. Based on the selected precursor parameters, the precursor parameters of the DUTs are collated into a one-dimensional vector, which will be used as part1 testing sample set. There are 35 sets of testing samples in part1 testing sample set. Since the testing conditions for each DUT have been already given in Table VI, only the corresponding material parameters and dimensional parameters are needed. Table IV shows the corresponding material parameters and dimensional parameters for each DUT.

The precursor parameters in the existing publications [42], [43], [44], [45], [46], [47], [48] are used as part2 testing sample set. There are 13 sets of testing samples in part2 testing sample set. Then, the same data preprocessing operation is performed for part1 and part2 testing sample sets. After the testing sample set is preprocessed, it is input into all the CNN classification models that are shown in Table III. The testing results of all the CNN classification models are given in Fig. 18. There are total 48 sets of testing samples in the testing sample set. From Fig. 18(a)–(c), it is shown that both the testing accuracies of best random CNN, CNN-1, and CNN-2 are lower than CNN-3. From Fig. 18(d), 26 sets of testing samples exhibit solder fatigue and 8 sets of testing samples exhibit bond wire lifting off, which is generally consistent with the PCT results. Three sets of lifting-off samples were misclassified. In addition, the bond wire heel crack samples and the "others" samples were completely correctly classified. That is, CNN-3 has the best performance of classification.

TABLE IV
CORRESPONDING MATERIAL PARAMETERS AND DIMENSIONAL PARAMETERS FOR EACH DUT

Precursor parameters	SKM50	FF100	SKM100	FF150
aspect ratio	0.2685	0.4	0.4	0.36
Diameter of bond wire (mm)	0.36	0.4	0.4	0.3
Chip and Solder Length (mm)	7.24	10.5	10.5	7.5
Chip and Solder Width (mm)	6.9	9.5	9.5	7.0
Chip Thickness (mm)	0.15	0.12	0.12	0.15
Solder Thickness (mm)	0.12	0.1	0.095	0.12
ΔCTE (between chip and solder layer)	20	20.5	20.5	22
ΔCTE (between chip and bond wire)	21	21	21	21

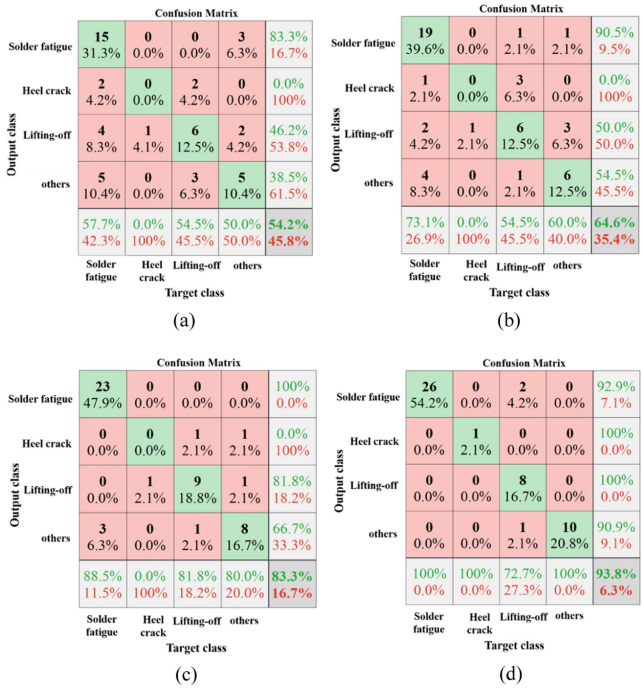

Fig. 18. Testing results of all the CNN classification models. (a) Best random CNN. (b) CNN-1. (c) CNN-2. (d) CNN-3.

TABLE V
TESTING ACCURACY AND ITS TIME CONSUMPTION COMPARISONS BETWEEN DIFFERENT ALGORITHMS

Optimizer	Intelligent Algorithms	Testing accuracy	Time consumption of testing
none	Best Random CNN	54.2%	6.112 s
The state-of-the-art PSO	CNN-1	64.6%	4.223 s
	CNN-2	83.3%	3.159 s
D-MPS-BP	CNN-3	93.8%	5.35 s
PSO	ELM	85.4%	0.0196 s
none	Gini index DT	87.5%	0.0138 s

Using the testing accuracy and the time consumption of testing as comparison indicators, the best random CNN, CNN-1, CNN-2, and CNN-3 are compared. We also provide testing results by using both PSO-ELM and Gini index DT. Table V gives corresponding comparison results.

First, the time consumptions of testing all CNN classification models are on the order of seconds. Second, the testing accuracy of CNN-3 is highest. That is, a well-trained CNN-3 classification model can quickly accomplish failure mode quad-classification with a highest classification accuracy. Finally, comparing CNN-2 and CNN-3, the testing accuracy of CNN-3 is higher. This is because both the architecture and hyperparameters of CNN-3 are optimized. This allows CNN-3 to be fully adapted to our quad-classification problem. For CNN-2, only the numbers of FC layers and the hyperparameters are optimized, and localized architecture is given manually. That is why CNN-2 cannot be adequately adapted to our quad-classification problem. For PSO-ELM and Gini index DT, although both intelligent algorithms have the advantage of less time cost, their classification accuracies are obviously lower than that of CNN-3.

V. CONCLUSION

In this article, an offline data-driven CNN-based classification method is proposed for failure mode quad-classification of different IGBT modules under different PCT conditions. This method consists of a training data collection part and a crucial hyperparameter optimization part. The training data collection part builds a training sample set (the largest to date) by mainly collecting various PCTs data from existing publications. This enables the proposed method robust enough to apply to different IGBT modules. The hyperparameter optimization part uses a joint search-type D-MPS-BP hyperparameter optimization method, which both uses a dynamic tuning strategy to try to avoid falling into a local optimum in each iteration, and an MPS to generate entirely new CNN architecture from scratch. Finally, PCTs of various IGBT under different PCT conditions are performed. The obtained PCT data and a small portion of the PCT data in the existing publications were used as testing sample set to verify the generalizability and robustness of the proposed method. The superiority of the proposed classification method is nicely demonstrated through the comparison with the random CNN, state-of-the-art PSO-CNN, PSO-ELM, and Gini index DT.

APPENDIX

TABLE VI
TESTING CONDITIONS OF PCTS

DUT	I_c(A)	t_{on}/t_{off} (s)	T_{jmax} (℃)	ΔT_j (℃)
DUT50-1-1	50	4/6	105	85
DUT50-1-2	50	4/6	120	85
DUT50-1-3	48	4/6	95	80
DUT50-2	58	2/3	140.76	95.7
DUT50-3-1	56	25/15	129	94
DUT50-3-2	56	25/15	132	96
DUT50-3-3	56	25/15	130	94
DUT50-3-4	56	25/15	131	96
DUT50-4-1	50	20/20	139.05	87.1
DUT50-4-2	50	20/20	135.8	83.6
DUT50-4-3	50	20/20	154.55	92.76
DUT50-4-4	50	20/20	151.5	90.3
DUT50-4-5	50	20/20	135.6	86.7
DUT50-4-6	50	20/20	135.06	83.3
DUT50-5-1	52.5	32/18	145.4	107.03
DUT50-5-2	52.5	32/18	147.9	103.3
DUT50-5-3	52.5	32/18	151.02	104.2
DUT50-5-4	52.5	32/18	160.73	112.7
DUT50-5-5	52.5	32/18	152.8	110
DUT50-5-6	52.5	32/18	157.4	112.7
DUT50-5-7	52.5	32/18	157.25	109.75
DUT50-5-8	52.5	32/18	160.9	112.7
DUT150-1-1	52	68/17	153.3	77
DUT150-1-2	52	68/17	155.5	79
DUT150-1-3	52	68/17	157.2	81
DUT150-1-4	52	68/17	157.9	81.7
DUT100-1-1	100	30/30	190	117
DUT100-1-2	100	30/30	190	128
DUT100-2-1	100	30/30	180	145
DUT100-2-2	100	30/30	190	141
DUT100-3-1	120	2/3	120	95
DUT100-3-2	120	2/3	124	100
DUT100-3-3	120	2/3	113	98
DUT100-3-4	120	2/3	122	94
DUT100-3-5	120	2/3	129	105

REFERENCES

[1] B. Ji et al., "In situ diagnostics and prognostics of solder fatigue in IGBT modules for electric vehicle drives," *IEEE Trans. Power Electron.*, vol. 30, no. 3, pp. 1535–1543, Mar. 2015, doi: 10.1109/TPEL.2014.2318991.

[2] F. Qin, X. Bie, T. An, J. Dai, Y. Dai, and P. Chen, "A lifetime prediction method for IGBT modules considering the self-accelerating effect of bond wire damage," *IEEE J. Emerg. Sel. Topics Power Electron.*, vol. 9, no. 2, pp. 2271–2284, Apr. 2021.

[3] P. D. Reigosa, H. Wang, Y. Yang, and F. Blaabjerg, "Prediction of bond wire fatigue of IGBTs in a PV inverter under a long-term operation," *IEEE Trans. Power Electron.*, vol. 31, no. 10, pp. 7171–7182, Oct. 2016, doi: 10.1109/TPEL.2015.2509643.

[4] X. Yang, Z. Lin, J. Ding, and Z. Long, "Lifetime prediction of IGBT modules in suspension choppers of medium/low-speed maglev train using an energy-based approach," *IEEE Trans. Power Electron.*, vol. 34, no. 1, pp. 738–747, Jan. 2019, doi: 10.1109/TPEL.2018.2812732.

[5] A. Hanif, Y. Yu, D. DeVoto, and F. Khan, "A comprehensive review toward the state-of-the-art in failure and lifetime predictions of power electronic devices," *IEEE Trans. Power Electron.*, vol. 34, no. 5, pp. 4729–4746, May 2019, doi: 10.1109/TPEL.2018.2860587.

[6] A. Abuelnaga, M. Narimani, and A. S. Bahman, "A review on IGBT module failure modes and lifetime testing," *IEEE Access*, vol. 9, pp. 9643–9663, 2021, doi: 10.1109/ACCESS.2021.3049738.

[7] K. B. Pedersen and K. Pedersen, "Dynamic modeling method of electro-thermo-mechanical degradation in IGBT modules," *IEEE Trans. Power Electron.*, vol. 31, no. 2, pp. 975–986, Feb. 2016, doi: 10.1109/TPEL.2015.2426013.

[8] Y. Lu and A. Christou, "Lifetime estimation of insulated gate bipolar transistor modules using two-step Bayesian estimation," *IEEE Trans. Device Mater. Rel.*, vol. 17, no. 2, pp. 414–421, Jun. 2017, doi: 10.1109/TDMR.2017.2694158.

[9] Y. Song and B. Wang, "Survey on reliability of power electronic systems," *IEEE Trans. Power Electron.*, vol. 28, no. 1, pp. 591–604, Jan. 2013.

[10] R. Reihanisaransari, F. Samadifam, A. A. Salameh, F. Mohammadiazar, N. Amiri, and S. Channumsin, "Reliability characterization of solder joints in electronic systems through a neural network aided approach," *IEEE Access*, vol. 10, pp. 123757–123768, 2022, doi: 10.1109/ACCESS.2022.3224008.

[11] V. Samavatian, M. Fotuhi-Firuzabad, M. Samavatian, P. Dehghanian, and F. Blaabjerg, "Iterative machine learning-aided framework bridges between fatigue and creep damages in solder interconnections," *IEEE Trans. Compon., Packag. Manuf. Technol.*, vol. 12, no. 2, pp. 349–358, Feb. 2022, doi: 10.1109/TCPMT.2021.3136751.

[12] V. Samavatian, M. Fotuhi-Firuzabad, M. Samavatian, P. Dehghanian, and F. Blaabjerg, "Correlation-driven machine learning for accelerated reliability assessment of solder joints in electronics," *Sci. Rep.*, vol. 10, no. 1, 2020, Art. no. 14821.

[13] L. Xie et al., "State-of-the-art of the bond wire failure mechanism and power cycling lifetime in power electronics," *Microelectron. Rel.*, vol. 147, 2023, Art. no. 115060.

[14] W. Liu, D. Zhou, F. Iannuzzo, M. Hartmann, and F. Blaabjerg, "Separation and validation of bond-wire and solder layer failure modes in IGBT modules," *IEEE Trans. Ind. Appl.*, vol. 58, no. 2, pp. 2324–2331, Mar./Apr. 2022, doi: 10.1109/TIA.2022.3141034.

[15] P. Melnyk, Z. You, and K. Li, "A high-performance CNN method for offline handwritten Chinese character recognition and visualization," *Soft Comput.*, vol. 24, no. 11, pp. 7977–7987, 2020.

[16] Y. Lecun, Y. Bengio, and G. Hinton, "Deep learning," *Nature*, vol. 521, no. 7553, pp. 436–444, 2015.

[17] M. Sahani and P. K. Dash, "FPGA-based deep convolutional neural network of process adaptive VMD data with online sequential RVFLN for power quality events recognition," *IEEE Trans. Power Electron.*, vol. 36, no. 4, pp. 4006–4015, Apr. 2021, doi: 10.1109/TPEL.2020.3023770.

[18] L. Wen, X. Li, and L. Gao, "A new reinforcement learning based learning rate scheduler for convolutional neural network in fault classification," *IEEE Trans. Ind. Electron.*, vol. 68, no. 12, pp. 12890–12900, Dec. 2021, doi: 10.1109/TIE.2020.3044808.

[19] R. Zhao, R. Yan, Z. Chen, K. Mao, P. Wang, and R. X. Gao, "Deep learning and its applications to machine health monitoring," *Mech. Syst. Signal Process.*, vol. 115, pp. 213–237, 2019.

[20] Y. Xia, Y. Xu, and B. Gou, "A data-driven method for IGBT open-circuit fault diagnosis based on hybrid ensemble learning and sliding-window classification," *IEEE Trans. Ind. Inform.*, vol. 16, no. 8, pp. 5223–5233, Aug. 2020, doi: 10.1109/TII.2019.2949344.

[21] W. Yu and C. Zhao, "Broad convolutional neural network based industrial process fault diagnosis with incremental learning capability," *IEEE Trans. Ind. Electron.*, vol. 67, no. 6, pp. 5081–5091, Jun. 2020, doi: 10.1109/TIE.2019.2931255.

[22] P. Probst, A. L. Boulesteix, and B. Bischl, "Tunability: Importance of hyperparameters of machine learning algorithms," *J. Mach. Learn. Res.*, vol. 20, no. 1, pp. 1934–1965, 2019.

[23] P. Singh, S. Chaudhury, and B. K. Panigrahi, "Hybrid MPSO-CNN: Multi-level particle swarm optimized hyperparameters of convolutional neural network," *Swarm Evol. Computation*, vol. 63, 2021, Art. no. 100863.

[24] Y. Wang, H. Zhang, and G. Zhang, "cPSO-CNN: An efficient PSO-based algorithm for fine-tuning hyper-parameters of convolutional neural networks," *Swarm Evol. Computation*, vol. 49, pp. 114–123, 2019.

[25] Q. Zhang, X. Zeng, W. Lo, and B. Fan, "Enterprise innovation evaluation method based on swarm optimization algorithm and artificial neural network," *Neural Comput. Appl.*, pp. 1–14, 2023.

[26] D. Tian and Z. Shi, "MPSO: Modified particle swarm optimization and its applications," *Swarm Evol. Computation*, vol. 41, pp. 49–68, 2018.

[27] K. Hu et al., "Cost-effective prognostics of IGBT bond wires with consideration of temperature swing," *IEEE Trans. Power Electron.*, vol. 35, no. 7, pp. 6773–6784, Jul. 2020.

[28] R. Schmidt and U. Scheuermann, "Separating failure modes in power cycling tests," in *Proc. Int. Conf. Integr. Power Electron. Syst.*, 2012, pp. 1–6.

[29] A. Otto, R. Dudek, K. Kolas, A. Mathew, C. Scherf, and S. Rzepka, "Modelling the lifetime of heavy wire-bonds in power devices–Concepts, limitations and challenges," in *Proc. IEEE 20th Intersociety Conf. Thermal Thermomechanical Phenomena Electron. Syst.*, 2021, pp. 670–678, doi: 10.1109/ITherm51669.2021.9503206.

[30] H. Wang, M. Su, and K. Sheng, "Theoretical performance limit of the IGBT," *IEEE Trans. Electron Devices*, vol. 64, no. 10, pp. 4184–4192, Oct. 2017, doi: 10.1109/TED.2017.2737021.

[31] M. H. Poech, "How materials behaviour affects power electronics reliability," in *Proc. 6th Int. Conf. Integr. Power Electron. Syst.*, 2010, pp. 1–6.

[32] M. Junghaenel, R. Schmidt, J. Strobel, and U. Scheuermann, "Investigation on isolated failure mechanisms in active power cycle testing," in *Proc. Int. Exhib. Conf. Power Electron., Intell. Motion, Renewable Energy Manage.*, 2015, pp. 1–8.

[33] H. Ma, M. Ahmad, and K.-C. Liu, "Reliability of lead-free solder joints under a wide range of thermal cycling conditions," *IEEE Trans. Compon., Packag. Manuf. Technol.*, vol. 1, no. 12, pp. 1965–1974, Dec. 2011, doi: 10.1109/TCPMT.2011.2171054.

[34] U.-M. Choi, F. Blaabjerg, and K.-B. Lee, "Study and handling methods of power IGBT module failures in power electronic converter systems," *IEEE Trans. Power Electron.*, vol. 30, no. 5, pp. 2517–2533, May 2015, doi: 10.1109/TPEL.2014.2373390.

[35] T. Ince, S. Kiranyaz, L. Eren, M. Askar, and M. Gabbouj, "Real-time motor fault detection by 1-D convolutional neural networks," *IEEE Trans. Ind. Electron.*, vol. 63, no. 11, pp. 7067–7075, Nov. 2016, doi: 10.1109/TIE.2016.2582729.

[36] C. W. Deng, L. Jiang, G. Gao, and Y. Huang, "Open-switch fault diagnosis of three-phase PWM converter systems for magnet power supply on EAST," *IEEE Trans. Power Electron.*, vol. 38, no. 1, pp. 1064–1078, Jan. 2023, doi: 10.1109/TPEL.2022.3194113.

[37] W. Yuan, Z. Li, Y. He, R. Cheng, L. Lu, and Y. Ruan, "Open-circuit fault diagnosis of NPC inverter based on improved 1-D CNN network," *IEEE Trans. Instrum. Meas.*, vol. 71, pp. 1–11, 2022, Art. no. 3510711, doi: 10.1109/TIM.2022.3166166.

[38] S. Mohaghegi, Y. del Valle, G. K. Venayagamoorthy, and R. G. Harley, "A comparison of PSO and backpropagation for training RBF neural networks for identification of a power system with STATCOM," in *Proc. IEEE Swarm Intell. Symp.*, 2005, pp. 381–384, doi: 10.1109/SIS.2005.1501646.

[39] Z. A. Bashir and M. E. El-Hawary, "Applying wavelets to short-term load forecasting using PSO-based neural networks," *IEEE Trans. Power Syst.*, vol. 24, no. 1, pp. 20–27, Feb. 2009, doi: 10.1109/TPWRS.2008.2008606.

[40] J. Kennedy and R. Eberhart, "Particle swarm optimization," in *Proc. Int. Conf. Neural Netw.*, 1995, vol. 4, pp. 1942–1948.

[41] Y. Huang, Y. Jia, Y. Luo, F. Xiao, and B. Liu, "Lifting-off of Al bonding wires in IGBT modules under power cycling: Failure mechanism and lifetime model," *IEEE J. Emerg. Sel. Topics Power Electron.*, vol. 8, no. 3, pp. 3162–3173, Sep. 2020, doi: 10.1109/JESTPE.2019.2924241.

[42] M. Bouarroudj, Z. Khatir, J. P. Ousten, F. Badel, L. Dupont, and S. Lefebvre, "Degradation behavior of 600 V–200 A IGBT modules under power cycling and high temperature environment conditions," *Microelectron. Rel.*, vol. 47, no. 9–11, pp. 1719–1724, 2007.

[43] Y. Zhao, E. Deng, M. Pan, Y. Zhang, and Y. Huang, "Influence of thermal coupling on lifetime under power cycling test," *IEEE Trans. Power Electron.*, vol. 37, no. 11, pp. 13641–13651, Nov. 2022.

[44] M. Hernes, S. D'Arco, O. C. Spro, and D. Peftitsis, "Improving monitoring of parallel ageing of IGBT bond-wires and solder layers by temperature compensation," in *Proc. Int. Exhib. Conf. Power Electron., Intell. Motion, Renewable Energy Manage.*, 2021, pp. 1–7.

[45] J. Lutz, T. Herrmann, M. Feller, R. Bayerer, T. Licht, and Raed Amro, "Power cycling induced failure mechanisms in the viewpoint of rough temperature environment," in *Proc. 5th Int. Conf. Integr. Power Electron. Syst.*, 2008, pp. 1–4.

[46] Y. Jia, Y. Huang, F. Xiao, H. Deng, Y. Duan, and F. Iannuzzo, "Impact of solder degradation on VCE of IGBT module: Experiments and modeling," *IEEE J. Emerg. Sel. Topics Power Electron.*, vol. 10, no. 4, pp. 4536–4545, Aug. 2022.

[47] A. Hensler, J. Lutz, M. Thoben, and K. Guth, "First power cycling results of improved packaging technologies for hybrid electrical vehicle applications," in *Proc. 6th Int. Conf. Integr. Power Electron. Syst.*, 2010, pp. 1–5.

[48] P. Seidel, C. Herold, J. Lutz, C. Schwabe, and R. Warsitz, "Power cycling test with power generated by an adjustable part of switching losses," in *Proc. 19th Eur. Conf. Power Electron. Appl.*, 2017, pp. P.1–P.10.

[49] S.-H. Tran et al., "Constant ΔTj power cycling strategy in DC mode for top-metal and bond-wire contacts degradation investigations," *IEEE Trans. Power Electron.*, vol. 34, no. 3, pp. 2171–2180, Mar. 2019.

[50] U. Scheuermann, R. Schmidt, and P. Newman, "Power cycling testing with different load pulse durations," in *Proc. 7th IET Int. Conf. Power Electron., Mach. Drives*, 2014, pp. 1–6.

[51] R. Schmidt, F. Zeyss, and U. Scheuermann, "Impact of absolute junction temperature on power cycling lifetime," in *Proc. 15th Eur. Conf. Power Electron. Appl.*, 2013, pp. 1–10.

[52] Y. Chen et al., "A comprehensive analytical and experimental investigation of wire bond life for IGBT modules," in *Proc. 27th Annu. IEEE Appl. Power Electron. Conf. Expo.*, 2012, pp. 2298–2304.

[53] A. Ibrahim et al., "Using of bond-wire resistance as aging indicator of semiconductor power modules," *Microelectron. Rel.*, vol. 114, 2020, Art. no. 113757.
[54] H. Huang and P. A. Mawby, "A lifetime estimation technique for voltage source inverters," *IEEE Trans. Power Electron.*, vol. 28, no. 8, pp. 4113–4119, Aug. 2013.
[55] L. Han, L. Liang, W. Xin, and F. Luo, "Influence of wire-bonding layout on reliability in IGBT module," in *Proc. 22nd Eur. Conf. Power Electron. Appl.*, 2020, pp. 1–7.
[56] J. Luo, S. Guan, B. Wan, M. Jiang, and G. Fu, "Research on IGBT bonding wires crack propagation at the macro and micro scales," *IEEE Access*, vol. 9, pp. 106270–106282, 2021.
[57] H. Lu, C. Bailey, and C. Yin, "Design for reliability of power electronics modules," *Microelectron. Rel.*, vol. 49, no. 9–11, pp. 1250–1255, 2009.
[58] Y. Celnikier, L. Benabou, L. Dupont, and G. Coquery, "Investigation of the heel crack mechanism in Al connections for power electronics modules," *Microelectron. Rel.*, vol. 51, no. 5, pp. 965–974, 2011.
[59] R. Schmidt, C. König, and P. Prenosil, "Novel wire bond material for advanced power module packages," *Microelectron. Rel.*, vol. 52, no. 9–10, pp. 2283–2288, 2012.
[60] K. C. Nwanoro, H. Lu, C. Yin, and C. Bailey, "An analysis of the reliability and design optimization of aluminium ribbon bonds in power electronics modules using computer simulation method," *Microelectron. Rel.*, vol. 87, pp. 1–14, 2018.
[61] C. Herold, J. Franke, R. Bhojani, A. Schleicher, and J. Lutz, "Requirements in power cycling for precise lifetime estimation," *Microelectron. Rel.*, vol. 58, pp. 82–89, 2016.
[62] K. Liu, J. Yang, J. Luo, L. Wang, Q. Huang, and F. Chen, "The characterization and application of chip topside bonding materials for power modules packaging: A review," *J. Phys.: Conf. Ser.*, vol. 1605, no. 1, 2020, Art. no. 012168.
[63] Y. Zhu, G. Li, R. Wang, S. Tang, H. Su, and K. Cao, "Intelligent fault diagnosis of hydraulic piston pump combining improved LeNet-5 and PSO hyperparameter optimization," *Appl. Acoust.*, vol. 183, 2021, Art. no. 108336.
[64] Y. Ma and Z. Zhang, "Travel mode choice prediction using deep neural networks with entity embeddings," *IEEE Access*, vol. 8, pp. 64959–64970, 2020, doi: 10.1109/ACCESS.2020.2985542.
[65] F. Han, H. F. Yao, and Q. H. Ling, "An improved evolutionary extreme learning machine based on particle swarm optimization," *Neurocomputing*, vol. 116, pp. 87–93, 2013.
[66] S. Tangirala, "Evaluating the impact of GINI index and information gain on classification using decision tree classifier algorithm," *Int. J. Adv. Comput. Sci. Appl.*, vol. 11, no. 2, pp. 612–619, 2020.
[67] M. C. Lai, L. Ran, O. Alatise, S. Xu, and P. Mawby, "Low ΔTj stress cycle effect in IGBT power module die-attach lifetime modeling," *IEEE Trans. Power Electron.*, vol. 31, no. 9, pp. 6575–6585, Sep. 2016, doi: 10.1109/TPEL.2015.2501540.
[68] S. Yang, D. Xiang, A. Bryant, P. Mawby, L. Ran, and P. Tavner, "Condition monitoring for device reliability in power electronic converters: A review," *IEEE Trans. Power Electron.*, vol. 25, no. 11, pp. 2734–2752, Nov. 2010, doi: 10.1109/TPEL.2010.2049377.
[69] M. Ciappa, "Selected failure mechanisms of modern power modules," *Microelectron. Rel.*, vol. 42, no. 4/5, pp. 653–667, 2002.

Xin Yang (Senior Member, IEEE) received the B.Eng. degree in electrical engineering and automation from the Huazhong University of Science and Technology, China, in 2009, the M.Sc. degree (with distinction) in analog and digital integrated circuit from Imperial College London, U.K., in 2010, and the Ph.D. degree in power electronics from the University of Cambridge, U.K., in 2014.

He is currently a full professor in Hunan University, China. His research interests mainly include power electronics, reliability of power electronic devices and underwater acoustic transducers.

Yue Zhang received the B.S. degree in electrical engineering from Xi'an University of Technology, Xi'an, China, in 2021. He is currently working toward the M.E. degree in electrical engineering with the College of Electrical and Information Engineering, Hunan University, Changsha, China.

His current research interests include reliability of power semiconductor devices.

Xinlong Wu received the B.S. degree in electric engineering from the Hefei University of Technology, Hefei, China, in 2017. He is currently working toward the Ph.D. degree in electrical engineering with the College of Electrical and Information Engineering, Hunan University, Changsha, China.

His current research interests include reliability of power semiconductor devices.

Guoyou Liu (Senior Member, IEEE) received the B.E. and M.E. degrees in physics from Wuhan University, Wuhan, China, in 1987 and 1990, respectively, and the Ph.D. degree in microelectronics from University of Chinese Academy of Sciences, Beijing, China, in 2017.

He joined China Railway Rolling Stock Corporation (CRRC), Beijing, China, in 1994. He is currently CRRC Scientist, and Executive Director of the State Key Laboratory of Advanced Power Semiconductor Device, Zhuzhou, China. He has been working on the technology development and industrialization of power semiconductors for more than 35 years. He has been supervising a number of national and provincial key projects, such as the 6-inch high-voltage Thyristor for ultra-high voltage dc power transmission, the 8-inch high-voltage IGBT chip and module development, the press-pack IGBT for HVDC application, and so on. He has authored or coauthored more than 90 journal papers and filed more than 200 patents with more than 120 of them granted. His current research interests include power semiconductor devices, modules, and system applications.